Asteroseismic modelling of solar-type stars: internal systematics from input physics and surface correction methods

B Nsamba, T Campante, M. J. P. F. G. Monteiro, M Cunha, B Rendle, D. Reese, K. Verma

Monthly Notices
of the
ROYAL ASTRONOMICAL SOCIETY

MNRAS **477,** 5052–5063 (2018)
Advance Access publication 2018 April 18

doi:10.1093/mnras/sty948

Asteroseismic modelling of solar-type stars: internal systematics from input physics and surface correction methods

B. Nsamba,[1,2]★ T. L. Campante,[1,2] M. J. P. F. G. Monteiro,[1,2] M. S. Cunha,[1,2] B. M. Rendle,[3,4] D. R. Reese[5] and K. Verma[4]

[1]*Instituto de Astrofísica e Ciências do Espaço, Universidade do Porto, Rua das Estrelas, P-4150-762 Porto, Portugal*
[2]*Departamento de Física e Astronomia, Faculdade de Ciências da Universidade do Porto, Rua do Campo Alegre, s/n, P-4169-007 Porto, Portugal*
[3]*School of Physics and Astronomy, University of Birmingham, Edgbaston, Birmingham B15 2TT, UK*
[4]*Stellar Astrophysics Centre, Department of Physics and Astronomy, Aarhus University, Ny Munkegade 120, DK-8000 Aarhus C, Denmark*
[5]*LESIA, Observatoire de Paris, PSL Research University, CNRS, Sorbonne Universités, UPMC Univ. Paris 06, Univ. Paris Diderot, Sorbonne Paris Cité, F-92195 Meudon, France*

Accepted 2018 April 12. Received 2018 April 12; in original form 2017 December 8

ABSTRACT

Asteroseismic forward modelling techniques are being used to determine fundamental properties (e.g. mass, radius, and age) of solar-type stars. The need to take into account all possible sources of error is of paramount importance towards a robust determination of stellar properties. We present a study of 34 solar-type stars for which high signal-to-noise asteroseismic data are available from multiyear *Kepler* photometry. We explore the internal systematics on the stellar properties, that is associated with the uncertainty in the input physics used to construct the stellar models. In particular, we explore the systematics arising from (i) the inclusion of the diffusion of helium and heavy elements; (ii) the uncertainty in solar metallicity mixture; and (iii) different surface correction methods used in optimization/fitting procedures. The systematics arising from comparing results of models with and without diffusion are found to be 0.5 per cent, 0.8 per cent, 2.1 per cent, and 16 per cent in mean density, radius, mass, and age, respectively. The internal systematics in age are significantly larger than the statistical uncertainties. We find the internal systematics resulting from the uncertainty in solar metallicity mixture to be 0.7 per cent in mean density, 0.5 per cent in radius, 1.4 per cent in mass, and 6.7 per cent in age. The surface correction method by Sonoi et al. and Ball & Gizon's two-term correction produce the lowest internal systematics among the different correction methods, namely, ∼1 per cent, ∼1 per cent, ∼2 per cent, and ∼8 per cent in mean density, radius, mass, and age, respectively. Stellar masses obtained using the surface correction methods by Kjeldsen et al. and Ball & Gizon's one-term correction are systematically higher than those obtained using frequency ratios.

Key words: asteroseismology – stars: evolution – stars: fundamental parameters – stars: oscillations.

1 INTRODUCTION

Our knowledge of the underlying physical processes taking place in deep stellar interiors is of great importance for the accurate characterization of stars and classification of stellar populations. The treatment and choice of the essential model input physics such as solar metallicity mixture (Grevesse & Sauval 1998; Asplund et al. 2009; Lodders & Palme 2009), initial helium abundance (Chiosi & Matteucci 1982; Casagrande et al. 2007), as well as the different mixing processes such as convection, semiconvection, convective overshooting (Monteiro, Christensen-Dalsgaard & Thompson 1996; Christensen-Dalsgaard et al. 2011; Deheuvels & Michel 2011; Piau et al. 2011; Silva Aguirre et al. 2011; Trampedach & Stein 2011), microscopic diffusion, radiation levitation, and rotational mixing (Thoul, Bahcall & Loeb 1994; Turcotte et al. 1998; Maeder & Meynet 2000) have a direct impact on the derived stellar parameters such as mass, radius, and age.

In order to aid the characterization of extra-solar planetary systems, current efforts are being geared towards improving the synergies between planetary science and asteroseismology (see e.g. the book by Campante, Santos & Monteiro 2017). Asteroseismology

★ E-mail: benard.nsamba@astro.up.pt

has proven to be an effective technique in determining precisely the exoplanet-host star parameters and hence planet properties (Huber et al. 2013; Benomar et al. 2014; Marcy et al. 2014; Campante et al. 2015, 2016a). Transit observations can only provide an estimate of the planet-to-star radius ratio. Therefore, precise stellar radii from asteroseismology allow tight constraints to be placed on the absolute sizes of the planets. For bright enough systems, radial-velocity observations may be combined with the transit data to estimate planetary masses. The inferred planetary mass scales with the stellar mass according to $M_{\rm p} \propto M^{2/3}$ (e.g. Perryman 2014) which asteroseismology can again provide (Campante et al. 2017). Last but not the least, stellar ages from asteroseismology can potentially be used to assess the dynamical stability of planetary systems and to establish their relative chronology.

Photometric observations by NASA's *Kepler* space telescope (Borucki et al. 2010) led to the characterization of several hundred solar-type stars using asteroseismology. Future space missions such as NASA's *Transiting Exoplanet Survey Satellite* (*TESS*; Campante et al. 2016b) will allow the detection of oscillations in up to 10 000 solar-type stars with low temporal resolution, whereas ESA's Planetary Transits and Oscillations of stars mission (PLATO; Rauer et al. 2014) is expected to reach ∼80 000 solar-type stars with detected oscillations based on multiyear observations. With this in mind, efforts are being directed towards increasing the precision of asteroseismic inferences by matching the observed oscillation frequencies (or their combinations) to the corresponding frequencies (or their combinations) obtained from the stellar evolutionary models (Miglio & Montalbán 2005; Metcalfe et al. 2012, 2014; Silva Aguirre et al. 2013, 2015; Davies et al. 2016). This approach is known to improve the precision of derived stellar parameters over forward modelling methods that only consider global oscillation parameters (i.e. the frequency of maximum oscillation power, $\nu_{\rm max}$, and the large frequency separation, $\Delta\nu$; Mathur et al. 2012; Lebreton & Goupil 2014). It nevertheless yields stellar parameters that are model dependent and therefore sensitive to the input physics used in the models. For instance, the estimated stellar ages are sensitive to different transport processes such as microscopic diffusion, convection, and overshooting, which need to be parametrized. Consequently, the treatment of the input physics becomes a source of uncertainty that cannot be easily accounted for.

Silva Aguirre et al. (2015) compared stellar properties of 33 *Kepler* planet-candidate host stars derived using a variety of stellar evolutionary codes and optimization/fitting methods, yielding internal systematics of ∼1 per cent in radius and density, ∼2 per cent in mass, and ∼7 per cent in age. In order to avoid internal systematics arising from the adoption of a variety of evolution and optimization tools, we employ the same tools in all computations performed in this work. This paper is then aimed at exploring systematic effects arising from specific choices of the input physics used in models of solar-type stars. In particular, we explore internal systematics[1] arising from the inclusion of diffusion in model grids and changes in element abundances. Inclusion of atomic diffusion in stellar models and its impact on the derived stellar parameters has been the subject of a number of studies over the past decades (Aller & Chapman 1960; VandenBerg et al. 2002; G88; G89; Dotter et al. 2017). This is mainly because atomic diffusion has been revealed to occur in the Sun and other stars (Guzik & Cox 1993; Christensen-Dalsgaard, Proffitt & Thompson 1993; Korn et al. 2007). We also explore the internal systematics arising from the uncertainty in the solar metallicity mixture. Different solar metallicity mixtures (e.g. Grevesse & Sauval 1998; Asplund et al. 2009) are being adopted in stellar modelling tools despite differences in the absolute element abundances (Miglio & Montalbán 2005; Serenelli & Basu 2010; Silva Aguirre et al. 2015, 2017). This hence becomes a potential source of uncertainty in the derived stellar parameters. Furthermore, we assess the internal systematics arising from commonly used surface correction methods. Ball & Gizon (2017) investigated the performance of different surface correction methods applied to the evolved stars (i.e. subgiants and low-luminosity red giants) and established the total additional uncertainties in the derived radii, masses, and ages to be less than 1 per cent, 2 per cent, and 6 per cent, respectively. In this paper, we assess the performance of different surface correction methods by comparing them with the use of frequency ratios, known to be less prone to near-surface effects (Roxburgh & Vorontsov 2003).

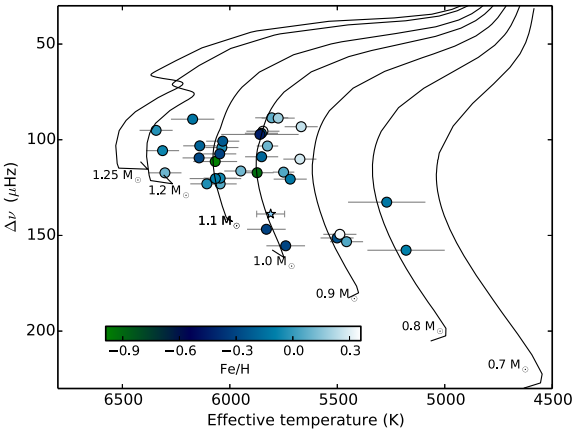

Figure 1. Target sample. Stellar evolutionary tracks were constructed at solar metallicity and range in mass from 0.7 to 1.25 $M_{\odot}$. Stars are colour-coded according to their metallicities. The 'star' symbol corresponds to the position of the Sun.

This paper is organized as follows. In Section 2, we describe our target sample, as well as the adopted seismic and spectroscopic observables. In Section 3, we present the stellar evolution code, the different model grids, and the optimization procedure used, while the main results are discussed in Section 4. Section 5 presents a summary of our findings.

2 TARGET SAMPLE

Our sample consists of 34 solar-type oscillators that have been observed by the *Kepler* satellite. Of these, 32 stars are part of the 'LEGACY' sample (Lund et al. 2017; Silva Aguirre et al. 2017) with the remaining two stars being the components of the asteroseismic binary HD 176465 (White et al. 2017; Nsamba et al. 2017). These stars were observed in *Kepler* short-cadence mode ($\Delta t = 58.89$ s) for at least 12 months. The sample includes some of the highest signal-to-noise ratio, solar-like oscillators observed by *Kepler*. Details about light-curve preparation, power spectrum calculation, the peak-bagging procedure, and adopted individual oscillation frequencies are given in Lund et al. (2017).

The target sample is shown in an asteroseismic Hertzsprung–Russell diagram in Fig. 1. The adopted $\Delta\nu$ is from Lund et al. (2017), computed following a Gaussian-weighted linear fit to $l = 0$

[1]Hereafter, we describe the internal systematics as the scatter, σ, induced on the derived stellar parameters from differences in the input physics or the surface correction method.

Table 1. Spectroscopic parameters of sample stars.

KIC	$T_{\rm eff}$ (K)	[Fe/H] (dex)
3427720	6045 ± 77	−0.06 ± 0.10
3656476	5668 ± 77	0.25 ± 0.10
3735871	6107 ± 77	−0.04 ± 0.10
4914923	5805 ± 77	0.08 ± 0.10
5184732	5846 ± 77	0.36 ± 0.10
5950854	5853 ± 77	−0.23 ± 0.10
6106415	6037 ± 77	−0.04 ± 0.10
6116048	6033 ± 77	−0.23 ± 0.10
6225718	6313 ± 77	−0.07 ± 0.10
6603624	5674 ± 77	0.28 ± 0.10
7106245	6068 ± 102[a]	−0.99 ± 0.19[a]
7296438	5775 ± 77	0.19 ± 0.10
7871531	5501 ± 77	−0.26 ± 0.10
8006161	5488 ± 77	0.34 ± 0.10
8150065	6173 ± 101[a]	−0.13 ± 0.15[a]
8179536	6343 ± 77	−0.03 ± 0.10
8379927	6067 ± 120[b]	−0.10 ± 0.15[b]
8394589	6143 ± 77	−0.29 ± 0.10
8424992	5719 ± 77	−0.12 ± 0.10
8760414	5873 ± 77	−0.92 ± 0.10
9025370	5270 ± 180[c]	−0.12 ± 0.18[c]
9098294	5852 ± 77	−0.18 ± 0.10
9139151	6302 ± 77	0.10 ± 0.10
9410862	6047 ± 77	−0.31 ± 0.10
9955598	5457 ± 77	0.05 ± 0.10
9965715	5860 ± 180[c]	−0.44 ± 0.18[c]
10079226	5949 ± 77	0.11 ± 0.10
10644253	6045 ± 77	0.06 ± 0.10
10963065	6140 ± 77	−0.19 ± 0.10
11772920	5180 ± 180[c]	−0.09 ± 0.18[c]
12069424	5825 ± 50[d]	0.10 ± 0.03[d]
12069449	5750 ± 50[d]	0.05 ± 0.02[d]

Note. The effective temperature ($T_{\rm eff}$) and metallicity ([Fe/H]) are adopted from [a]Casagrande et al. (2014), [b]Pinsonneault et al. (2012),[c]Pinsonneault et al. (2014), and [d]Ramírez, Meléndez & Asplund (2009) as indicated. The remaining parameters are from Lund et al. (2017).

mode frequencies expressed as a function of the radial order. Most of the stars in the target sample are more evolved than the Sun. Table 1 contains the atmospheric properties of the stars in our sample. Most of the spectroscopic parameters were retrieved from Lund et al. (2017). These classical constraints will complement the asteroseismic parameters in the optimization procedure (as described in Section 3). The components of the binary HD 176465 (White et al. 2017) have effective temperatures 5830 ± 90 K (HD 176465 A) and 5740 ± 90 K (HD 176465 B), and similar metallicity (−0.30 ± 0.06 dex).

3 STELLAR MODELS AND FITTING PROCEDURE

We describe the stellar evolution code adopted in this work and the physics used in the construction of the different grids in Section 3.1, while the adopted optimization/fitting procedure is described in Section 3.2.

3.1 Grid construction

We used the 1D stellar evolution code Modules for Experiments in Stellar Astrophysics (MESA; Paxton et al. 2011, 2013, 2015) to generate grids of main-sequence and subgiant stellar models. The evolutionary tracks were varied in mass, M, initial metal mass fraction, Z, and mixing length parameter, $\alpha_{\rm mlt}$ (Böhm-Vitense 1958). The parameter ranges are: $M \in [0.70, 1.25]\,{\rm M}_{\odot}$ in steps of $0.05\,{\rm M}_{\odot}$, $Z \in [0.006, 0.031]$ in steps of 0.001, and $\alpha_{\rm mlt} \in [1.3, 2.9]$ in steps of 0.1. In our grids, neither convective overshoot nor semiconvection was included. Stellar models with masses $\gtrapprox 1.1\,{\rm M}_{\odot}$ (at solar metallicity) are expected to have convective cores while on the main sequence and core overshoot may therefore be an important aspect to consider in the construction of a grid. Most of our target stars have masses below this mass limit. The impact of including core overshoot is beyond the scope of this study and it has not been included in our grids. In two of the grids (see Table 2), element diffusion was included according to Thoul et al. (1994) to allow for diffusion of hydrogen and gravitational settling of heavy elements (i.e. ^{4}He, ^{16}O, and ^{56}Fe). No radiative levitation was included in the models.

Specifically, we used MESA version 7624, whose equation of state works with density, ρ, and temperature, T, as independent natural variables in a Helmholtz free energy formulation of thermodynamics. The basic input physics used in all of our grids includes the 2005 updated version of the OPAL equation of state (Rogers & Nayfonov 2002). The stellar models used opacities from OPAL tables (Iglesias & Rogers 1996) at high temperatures, whereas at lower temperatures tables from Ferguson et al. (2005) were used instead. Nuclear reaction rates were obtained from tables provided by the NACRE collaboration (Angulo et al. 1999). Specific rates for $^{14}{\rm N}(p,\gamma)^{15}{\rm O}$ were from Imbriani et al. (2005) and for $^{12}{\rm C}(\alpha,\gamma)^{16}{\rm O}$ from Kunz et al. (2002). The standard Grey–Eddington atmosphere was used to integrate the atmospheric structure from the photosphere to an optical depth of 10^{-4}. The initial helium mass fraction, Y, of our evolution models was determined using the helium-to-heavy metal enrichment law anchored to the big bang nucleosynthesis values of $Z_0 = 0.0$ and $Y_0 = 0.2484$ (Cyburt, Fields & Olive 2003). We therefore define the initial helium mass fraction according to

$$Y = \left(\frac{\Delta Y}{\Delta Z}\right) Z + Y_0. \quad (1)$$

The enrichment law ratio, $\Delta Y/\Delta Z$, ranges from 1 to 3 based on both theoretical and observational studies (Jimenez et al. 2003; Balser 2006; Casagrande et al. 2007; Serenelli & Basu 2010). Typically, a value of $\Delta Y/\Delta Z$ determined through a solar calibration is adopted in equation (1). This would mean that stars in the sample are assumed to have formed in regions having the same helium-to-heavy element mass fraction as the Sun. In order to avoid any systematics that could arise from variations in the treatment of the initial helium mass fraction, we set $\Delta Y/\Delta Z = 2$ (Chiosi & Matteucci 1982; Casagrande et al. 2007) in all of our grids. The systematic contributions arising from the treatment of initial helium mass fraction will be addressed in a separate paper.

The grids were evolved starting from the pre-main sequence (PMS) to the zero-age main sequence (ZAMS). We define the ZAMS as the point along the evolutionary track where the nuclear luminosity of the model yields 90 per cent of the total luminosity. All PMS models were discarded since our target stars are more evolved. We then evolved the models from the ZAMS to the point along the evolutionary track where $\log \rho_{\rm c} = 4.5$ ($\rho_{\rm c}$ is the central density). This approximately corresponds to the base of the red giant branch. About 70 models were stored at different ages along each evolutionary track and a total of about 371 280 models for each grid. For each model, we used GYRE (Townsend & Teitler 2013) in its adiabatic setting to generate theoretical oscillation frequencies. Pressure-mode (p-mode) oscillation frequencies were computed for

Table 2. Summary of adopted grids.

Name	Mass range ($M_\odot$)	Solar metallicity mixture	$\frac{\Delta Y}{\Delta Z}$	Overshoot	Diffusion
GS98sta	0.70–1.25	Grevesse & Sauval (1998)	2.0	No	Yes
GS98nod	0.70–1.25	Grevesse & Sauval (1998)	2.0	No	No
AGS09	0.70–1.25	Asplund et al. (2009)	2.0	No	Yes

harmonic degrees $l = 0$, 1, 2, and 3 below the acoustic cut-off frequency.

It is worth noting that an offset is always seen between model and observed frequencies (Christensen-Dalsgaard, Dappen & Lebreton 1988; Dziembowski, Paterno & Ventura 1988; Christensen-Dalsgaard & Thompson 1997). This is due to an improper modelling of the near-surface layers. In order to model convection, the mixing-length theory is often used, which is only valid in the deep stellar interior and does not properly describe convection near the surface. In addition, the description of the interaction between oscillations and convection is still poorly understood. Also, other active processes such as magnetic fields affect the properties of the oscillations and the equilibrium structure, however, their inclusion in the modelling is challenging and thus usually neglected. Altogether, these give rise to a surface effect not properly accounted for in the models, hence becoming a substantial obstacle to the direct comparison of model frequencies with observed frequencies. The surface effect in our model frequencies was corrected using various surface correction methods (see Section 4.3) and implemented in the optimization tool (as described in Section 3.2).

3.2 Optimization procedure

Asteroseismic Inference on a Massive Scale[2] (AIMS; Rendle et al. in preparation) is based on a Bayesian approach and generates probability distribution functions (PDFs) of the different stellar parameters. In order to generate a representative set of models reproducing a specified set of asteroseismic and classical constraints, AIMS uses a Markov chain Monte Carlo algorithm based on Foreman-Mackey et al. (2013) in combination with interpolation based on a Delaunay tessellation of the stellar grid. With A representing different stellar parameters and O various asteroseismic and classical observables, from Bayes theorem one has

$$p(A|O) \propto p(O|A)\, p(A), \tag{2}$$

where $p(A)$ denotes our prior assumptions. We assigned uniform prior distributions to M, Z, and $\alpha_{\rm mlt}$. Given a set of model parameters, the likelihood of obtaining a set of observables is given by (see e.g. the book by Gregory 2005)

$$p(O|A) = \frac{1}{(2\pi)^{\frac{1}{2}}\sqrt{|C|}} \exp(-\chi^2/2), \tag{3}$$

where C is the covariance matrix of the observed parameters. It is worth noting that we assumed Gaussian distributed errors for our observables (i.e. individual oscillation frequencies, effective temperature, and metallicity). When dealing with independent observables, then χ^2 is defined as

$$\chi^2 = \sum_{i=1}^{N} \left(\frac{O_i - \theta_i}{\sigma_i} \right)^2, \tag{4}$$

[2] http://bison.ph.bham.ac.uk/spaceinn/aims/

where O_i, θ_i, and σ_i are the observed value, modelled value, and the associated observed uncertainties, respectively. When one instead fits frequency ratios (Section 4.3), correlations will be introduced that are a function of frequency. This is taken into account in the likelihood function (equation 3) and, in this case, the χ^2 of each model is given by (e.g. Gregory 2005)

$$\chi^2 = (O - \theta)^T C^{-1} (O - \theta). \tag{5}$$

We stress that the frequency ratios used in this paper were calculated using AIMS. We further complemented the frequency ratios with the large frequency separation calculated from $l = 0$ modes as seismic constraints. Furthermore, we note that we give equal weights to the seismic and classical constraints during the computation of total χ^2. Finally, the different stellar parameters and their uncertainties are obtained from the statistical mean and standard deviation of the posterior PDFs.

4 RESULTS AND DISCUSSION

We discuss in detail the different input physics under investigation in Sections 4.1 and 4.2. It should be noted that some inputs cannot be examined separately since their modification requires changing other inputs. For instance, modifications in the solar metallicity mixture require setting the corresponding appropriate opacities. Therefore, in such cases, the systematics found are from both sets of inputs. The two-term surface correction method by Ball & Gizon (2014) is used to obtain the results presented in Sections 4.1 and 4.2. In Section 4.3, we used the GS98sta grid in the analysis of the internal systematics arising from using different frequency correction methods. The percentage median statistical uncertainties obtained when using the reference grid GS98sta are 0.3 per cent in mean density, 0.6 per cent in radius, 1.6 per cent in mass, and 7.4 per cent in age (see Fig. 2).

4.1 Diffusion

Atomic diffusion (or element diffusion) is a transport process that occurs in radiative regions of stars. It can be driven by temperature gradients (thermal diffusion), gravity or pressure gradients (gravitational settling), and composition gradients (chemical diffusion). Thermal diffusion and gravitational settling, concentrate heavier elements towards the centre of the star (Thoul et al. 1994). These two processes are opposed by composition gradients. Atomic diffusion is a less-efficient process in convective regions since convection is a highly vigorous process that occurs on shorter time-scales. Diffusion requires a quiet environment so that settling is not prevented by large-scale motions (Chaboyer et al. 2001). We switch on element diffusion in MESA, which includes chemical diffusion and gravitational settling (Paxton et al. 2011). MESA's diffusion module uses diffusion coefficients from Thoul et al. (1994) in order to solve Burger's equations when calculating particle diffusion and gravitational settling.

Fig. 3 (left-hand panel) shows that stellar ages derived using GS98nod are systematically larger than those derived using

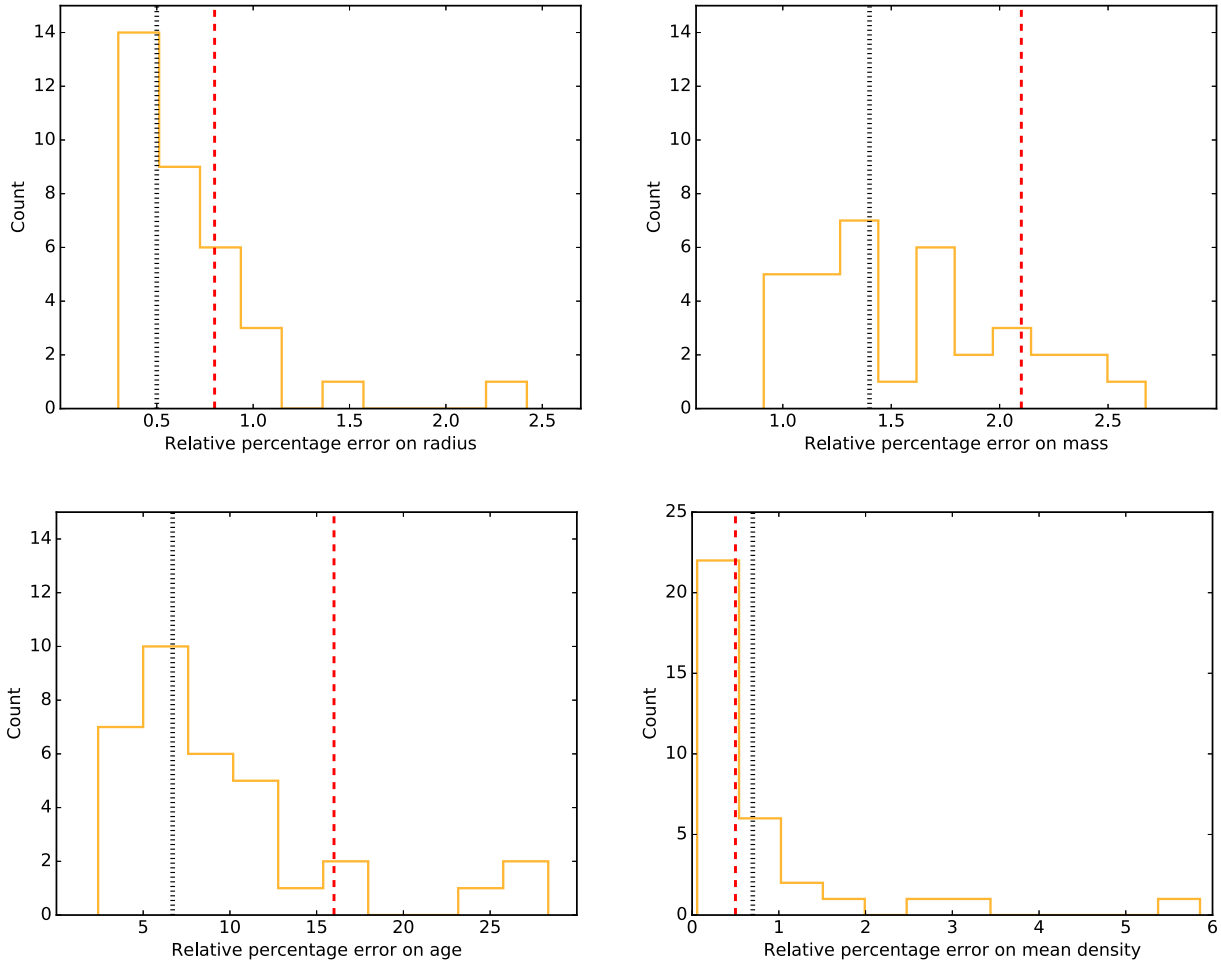

Figure 2. Statistical uncertainties and internal systematics. Histograms represent the distributions of statistical uncertainties when adopting the reference grid GS98sta. Black dotted lines represent internal systematic contributions from AGS09 (composition). Red dashed lines represent internal systematic contributions from GS98nod (diffusion).

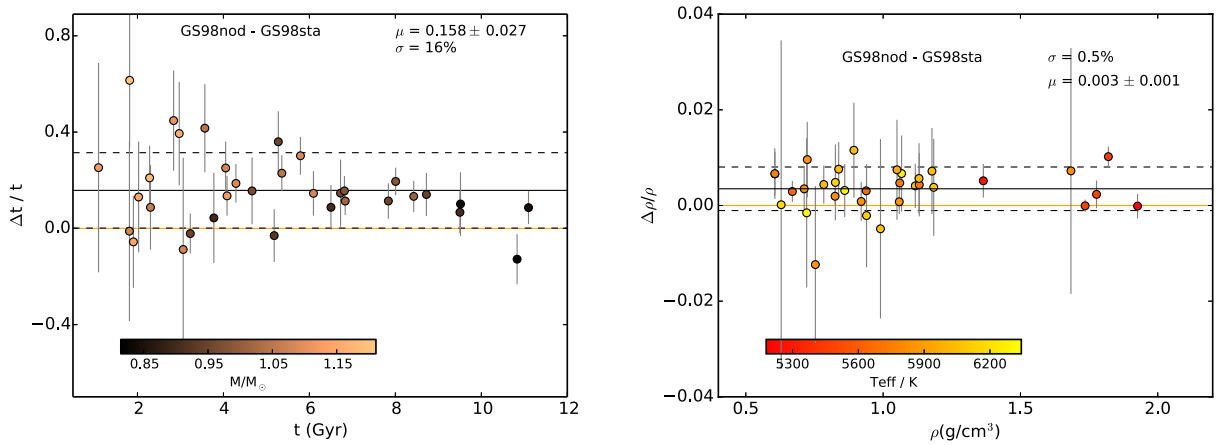

Figure 3. Fractional difference in age (left) and mean density (right) as a function of GS98sta stellar parameters. The colour-coding is with respect to the stellar mass and the effective temperature for the left-hand and right-hand panels, respectively. The solid black line indicates the bias (μ), while the scatter (σ) is represented by the dashed lines. The zero level is represented by the solid orange line.

GS98sta. In our optimization process, we use the effective temperature and metallicity as classical observables. Since element diffusion changes surface element abundance, our GS98sta grid will need to have best-fitting models with higher initial metal mass fractions so that the surface metal mass fractions can be comparable to the observed values at the stars' current ages. This implies that the opacity in the cores of these models will be higher throughout their evolution, compared to the case of no diffusion. To avoid the associated

decrease in luminosity, which is indirectly constrained by the effective temperature and seismic data, the best-fitting models need to have higher mass, justifying their younger age. This is confirmed in Fig. 4 (left-hand panel) where we show the fractional differences in the stellar mass. In turn, the strong constraints on the mean density imposed by the seismic data lead to an increase in the radius of the best-fitting models in our GS98sta grid, as shown in Fig. 4 (right-hand panel). In summary, in order to satisfy the observables, models with diffusion need to have higher masses, hence also higher radii and younger ages.

We explore internal systematics by comparing models with and without diffusion, resulting in 0.5 per cent, 0.8 per cent, 2.1 per cent, and 16 per cent in mean density, radius, mass, and age, respectively (see Figs 3 and 4). The internal systematics in density, mass, and radius are comparable to their statistical uncertainties, while the internal systematics in age are significantly larger than the statistical uncertainties (See Fig. 2).

Furthermore, we inspect the data presented in both Figs 3 and 4 for the presence of linear correlations. We employ a correlation coefficient analysis developed in a Bayesian framework (Figueira et al. 2016). Using it we can estimate the posterior probability distribution of the correlation coefficient. Table 3 shows the results from such Bayesian test. At the 95 per cent confidence level, there is a negative linear trend present for the radius and mass, with a hint of a similar trend being present for the age. The difference between the initial and current metal mass fraction, Z, of the best-fitting models of GS98sta increases with increasing stellar mass. This suggests that gravitational settling has a larger impact on higher mass stars, explaining the trend with mass seen in Fig. 4.

4.2 Composition

Solar metallicity mixtures are one of the most important ingredients in stellar modelling. Here we focus on the most commonly used solar metallicity mixtures in constructing standard solar models, namely, those from Grevesse & Sauval (1998) and Asplund et al. (2009). We define [Fe/H] in all our calculations as

$$[\mathrm{Fe/H}] = \log\left(\frac{Z_{\mathrm{surface}}}{X_{\mathrm{surface}}}\right)_{\mathrm{star}} - \log\left(\frac{Z_{\mathrm{surface}}}{X_{\mathrm{surface}}}\right)_{\odot}, \tag{6}$$

where X_{surface} and Z_{surface} refer to the surface hydrogen and heavy element mass fractions, respectively. We used solar Z_{surface} values of 0.0134 and 0.0169 based on Asplund et al. and Grevesse & Sauval, respectively. In general, the solar metallicity mixture from AGS09 is lower than those from GS98sta. Basu & Antia (2004) demonstrate that the uncertainty in solar metallicity mixture results in differences in the sound speed in the stellar interiors.

We assess the internal systematics arising from the uncertainty in solar metallicity mixture. We find a good agreement in both the derived ages and densities with internal systematics of 6.7 per cent (with a bias of 0.013 ± 0.012) and 0.7 per cent (with a bias of 0.002 ± 0.001), respectively (see Fig. 5). Internal systematics in stellar ages are somewhat smaller than the statistical uncertainties (median of 7.4 per cent) as shown in Fig. 2. Furthermore, we find internal systematics of 0.5 per cent in radius and 1.4 per cent in mass (see Fig. 6). Silva Aguirre et al. (2015) found systematic contributions arising from the uncertainty in solar metallicity mixture to be 0.3 per cent in mean density and radius, 0.6 per cent in mass, and 3.3 per cent in age. The internal systematics found in this work are approximately twice as large as those found by Silva Aguirre et al. (2015). The most probable cause for this discrepancy is in the treatment of the mixing length parameter (α_{mlt}). In this paper, we set α_{mlt} as a free variable in all of our grids (see Section 3.1), while Silva Aguirre et al. (2015) used solar calibrated α_{mlt} values. We note that the uncertainty in solar metallicity mixture will cause variations in solar calibrated values of α_{mlt}. Systematic uncertainties arising from grids varying in the treatment of α_{mlt} were found to be 0.7 per cent, 0.6 per cent, 2.2 per cent, and 9.0 per cent in mean density, radius, mass, and age, respectively (Silva Aguirre et al. 2015). In addition, based on a grid of 3D convection simulations, α_{mlt} has been shown to span a range of values on the main sequence (Trampedach et al. 2014). It is therefore advisable to use a range of α_{mlt} values when constructing stellar grids for the Sun-like stars.

4.3 Surface correction

To overcome the well-known systematic differences between model and observed oscillation frequencies (Section 3), several surface correction methods have been put forward (see Table 4). The function, f, used in the different surface correction methods is given by

$$f = \frac{\nu}{\nu_0}, \tag{7}$$

where ν is the mode oscillation frequency and ν_0 a reference frequency. When using surface correction method proposed by Sonoi et al. (2015), the value of ν_0 is determined in AIMS by means of the scaling relation (Brown et al. 1991; Kjeldsen & Bedding 1995):

$$\nu_0 = \left(\frac{M}{M_{\odot}}\right)\left(\frac{R}{R_{\odot}}\right)^{-2}\left(\frac{T_{\mathrm{eff}}}{T_{\mathrm{eff},\odot}}\right)^{-1/2}\nu_{\mathrm{max},\odot}. \tag{8}$$

The adopted solar values are $\nu_{\mathrm{max},\odot} = 3104.0$ μHz, $R_{\odot} = 6.9599 \times 10^{10}$ cm, $M_{\odot} = 1.98919 \times 10^{33}$ g, and $T_{\mathrm{eff},\odot} = 5777.0$ K (Allen 1976; Mamajek 2012; Mosser et al. 2013). For other surface corrections, we used

$$\nu_0 = \frac{1}{2\pi}\sqrt{\frac{GM}{R}}, \tag{9}$$

where G and R are the gravitational constant and model radius, respectively. This does not make a difference on the correction, but only affects the magnitude of the fitting coefficients (i.e. a and b). Some striking differences between the different surface correction methods are worth mentioning. Kjeldsen, Bedding & Christensen-Dalsgaard (2008) proposed that the offset depends on a power of the mode frequency, whose exponent, b, is determined to be $b = 4.9$ (calibrated with respect to solar data). The same value has subsequently been adopted in the study of other stars (Metcalfe et al. 2010; Brandão et al. 2011; Van Eylen et al. 2012; Gruberbauer et al. 2013). Using Canuto–Goldman–Mazzitelli modelling of convection, Deheuvels et al. (2014) determined a value of b to be 4.25 and adopted it in generating models using the CESAM2k evolutionary code. We adopted the former value of b in AIMS when using the surface correction of Kjeldsen et al. (2008), as shown in Table 4. Sonoi et al. (2015) established that the power-law function proposed by Kjeldsen et al. (2008) is not satisfactory in fitting the high-frequency range. This was attributed to the nature of the profile of the frequency difference, $\delta\nu$, which becomes less steep as the frequency increases beyond ν_{max}. Sonoi et al. (2015) thus proposed a Lorentzian function that they found to better fit in the profile of the frequency difference across the whole frequency range. It should be noted that the modified Lorentzian function proposed by Sonoi et al. (2015) reduces to the equation proposed by Kjeldsen et al. (2008), when $f \ll 1$. Furthermore, the scaling factor, r, related to the mean density and proposed by Kjeldsen et al. (2008), is not

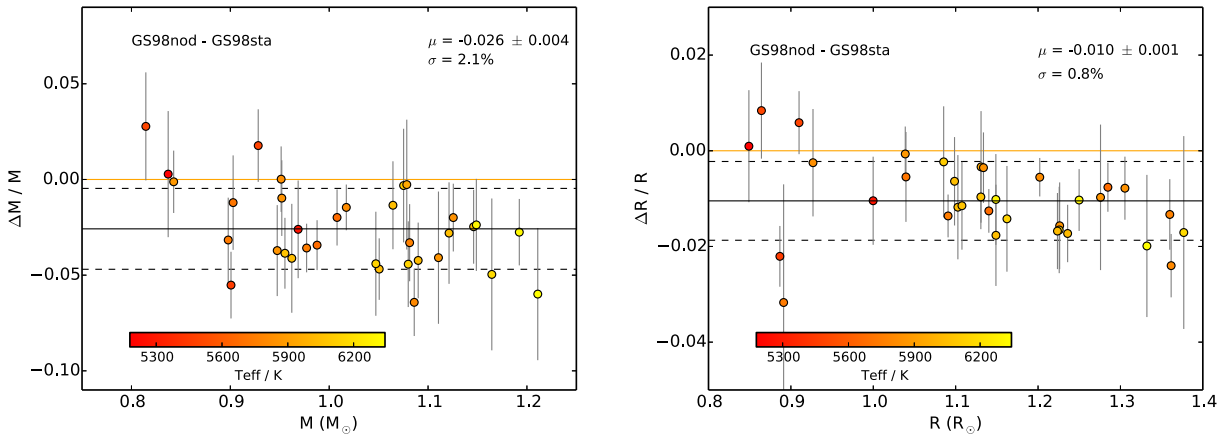

Figure 4. Fractional difference in mass (left) and radius (right) as a function of GS98sta stellar parameters. The zero level is represented by the solid orange line. The colour-coding is with respect to the effective temperature. The solid black line indicates the bias (μ), while the scatter (σ) is represented by the dashed lines.

Table 3. Statistical summary of the posterior probability distribution of the correlation coefficient. C.I. denotes the confidence interval.

Parameter	Mean	Standard deviation	95 per cent C.I.
Mass	−0.433	0.135	[−0.69, −0.168]
Radius	−0.342	0.142	[−0.599, −0.049]
Age	−0.247	0.152	[−0.535, 0.047]

used in AIMS. The risk with rescaling the model is that one will need to change a number of variables (e.g. how is heat transport affected). It may be possible to rescale the acoustic variables consistently, but other variables may not remain consistent. Hence, for this reason the *r*-scaling is not implemented in AIMS. If there is a mismatch, then AIMS looks for another model where the mean density is closer, rather than trying to rescale the model to the right mean density. Ball & Gizon (2014) proposed two functions (BG1 and BG2, see Table 4), both taking into account the mode inertia, *I*. This was based on findings of Gough (1990) and Goldreich et al. (1991) who argued that perturbations caused by a magnetic field would cause changes proportional to ν^3/I and a change in the description of convection is expected to cause changes proportional to ν^{-1}/I. BG1 takes into account only the cubic term while BG2 combines both terms (see Table 4).

We note that we used the same set of observed frequencies for each star when applying the different surface correction methods during the optimization process. This is because we aimed at carrying out a uniform analysis for all the different surface correction methods.

We explore the internal systematics from adopting the different surface correction options by comparing the model parameters derived in each case with those obtained when using frequency ratios. Frequency ratios have been shown to be less affected by the poorly modelled surface layers and this permits direct comparison of observed oscillation frequencies with the theoretical oscillations frequencies without applying any surface correction routine (Roxburgh & Vorontsov 2003; Silva Aguirre et al. 2011, 2015, 2017). Unfortunately, some information about the star is lost when one uses frequency ratios. For instance, since the stellar mean density scales with the frequencies, taking frequency ratios results into factoring out the mean density and thus making frequency ratios less sensitive to the mean density compared to direct comparison with the oscillation frequencies (Roxburgh & Vorontsov 2003). Despite this, frequency ratios have been reported to constrain stellar interiors, resulting in a more precise asteroseismic stellar ages compared to the use of individual frequencies. In AIMS, we specified the frequency ratios r_{10}, r_{01}, and r_{02} as (Roxburgh & Vorontsov 2003):

$$r_{01}(n) = \frac{d_{01}(n)}{\Delta\nu_1(n)}, \quad r_{10}(n) = \frac{d_{10}(n)}{\Delta\nu_0(n+1)}, \tag{10}$$

$$r_{02}(n) = \frac{d_{02}(n)}{\Delta\nu_1(n)}, \tag{11}$$

where $\Delta\nu_l(n) = \nu_{n,l} - \nu_{n-1,l}$ is the large frequency separation, n is the mode radial order, l is the mode harmonic degree, and $d_{02}(n) = \nu_{n,0} - \nu_{n-1,2}$ is the small frequency separation. Moreover, $d_{01}(n)$ and $d_{10}(n)$ are defined as

$$d_{01}(n) = \frac{1}{8}(\nu_{n-1,0} - 4\nu_{n-1,1} + 6\nu_{n,0} - 4\nu_{n,1} + \nu_{n+1,0}), \tag{12}$$

$$d_{10}(n) = -\frac{1}{8}(\nu_{n-1,1} - 4\nu_{n,0} + 6\nu_{n,1} - 4\nu_{n+1,0} + \nu_{n+1,1}). \tag{13}$$

Hereafter, the surface correction method by Kjeldsen et al. (2008) is denoted by KJ, Sonoi et al. (2015) as Sonoi, Ball & Gizon (2014) one-term correction as BG1, and Ball & Gizon (2014) two-term correction as BG2 (See Table 4). Sonoi and BG2 lead to smaller internal systematics in mass: 2.0 per cent and 1.7 per cent, respectively (see Fig. 7). We find that the masses are overestimated when employing the corrections by KJ and BG1. KJ also yields internal systematics of 2.0 per cent in mass, albeit affected by a larger bias of 0.029 ± 0.004. All surface correction routines yield similar internal systematics in radius, with BG1 leading to the largest bias (see Fig. 8). Both KJ and BG2 produce internal systematics in radius of 0.8 per cent, while Sonoi yields 0.9 per cent. Fig. 9 shows that Sonoi and BG2 produce smaller internal systematics in age: 8.2 per cent and 7.2 per cent, respectively. KJ results in internal systematics of 10 per cent, while BG1 yields the largest internal systematics (19.4 per cent).

BG2 yields the least median reduced χ^2_ν in the model-to-observed frequency differences of 5.661. Sonoi and KJ yield comparable median reduced χ^2_ν of 15.846 and 15.958, respectively. BG1 gives median reduced χ^2_ν of 27.800. This in turn explains why

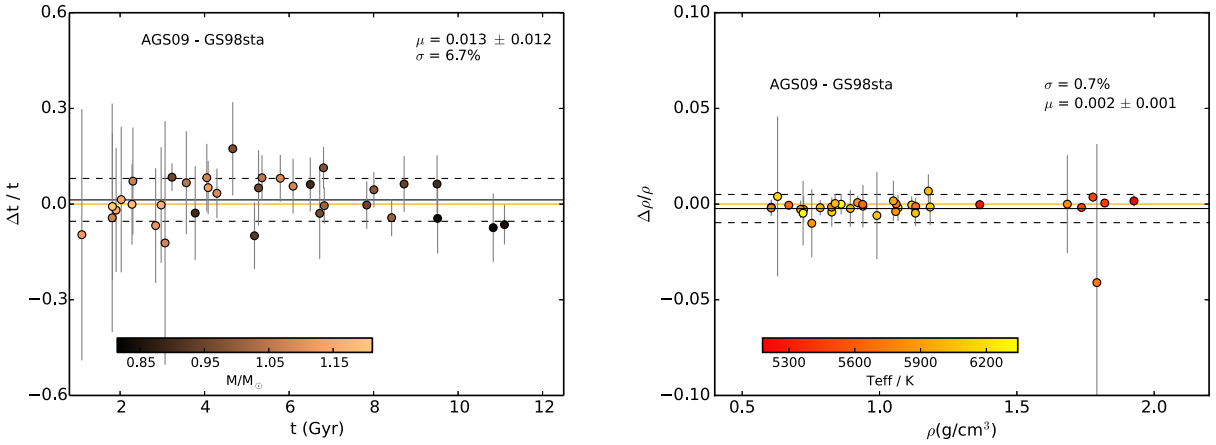

Figure 5. Fractional difference in age (left) and mean density (right) as a function of GS98sta stellar parameters. The colour-coding is with respect to the stellar mass. The zero level is represented by the solid orange line. The solid black line indicates the bias (μ), while the scatter (σ) is represented by the dashed lines.

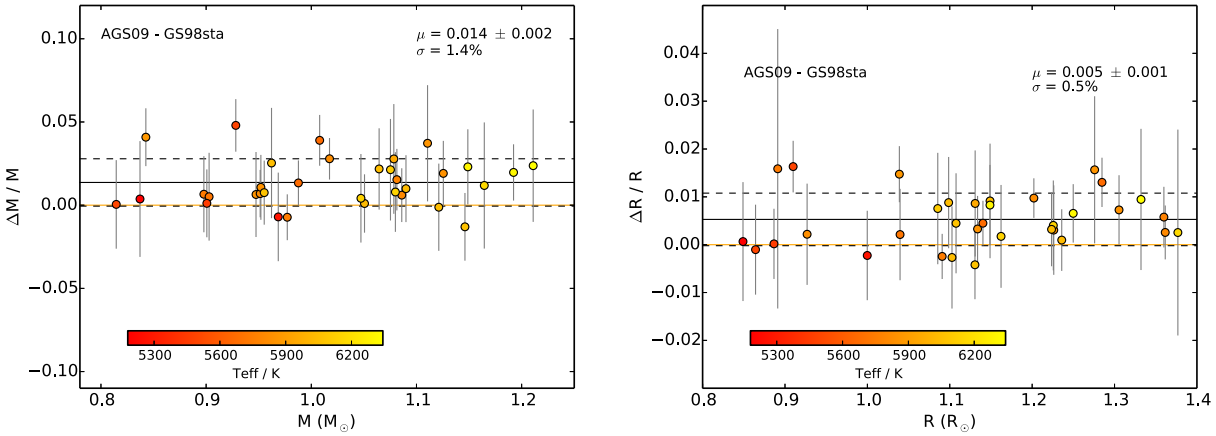

Figure 6. Fractional difference in mass (left) and radius (right) as a function of GS98sta stellar parameters. The zero level is represented by the solid orange line. The colour-coding is with respect to the effective temperature. The solid black line indicates the bias (μ), while the scatter (σ) is represented by the dashed lines.

Table 4. Summary of the different surface correction methods. a and b are best-fitting parameters (see the text for details), f is a function that depends on the mode frequency, I is the normalized mode inertia, and $\delta\nu$ is the offset between observed and model frequencies.

Name	Functions	b-value	Reference
KJ	$\delta\nu = af^b$	4.9	Kjeldsen et al. (2008)
BG1	$\delta\nu = af^3/I$	–	Ball & Gizon (2014)
BG2	$\delta\nu = (af^{-1} + bf^3)/I$	–	Ball & Gizon (2014)
Sonoi	$\delta\nu = a\left(1 - \frac{1}{1+f^b}\right)$	4.0	Sonoi et al. (2015)

the BG2 leads to the least internal systematics followed by Sonoi.

In Fig. 10, we consider BG2 results as the reference in the comparison with the different surface correction methods. This is because from Figs 7, 8, and 9, BG2 yields the least internal systematics in mass, radius, and age, respectively. In addition, frequency ratios will provide a poor description of the near-surface layers. It can clearly be seen in Fig. 10 that some information about the mean density is lost when one uses frequency ratios. Since we used uncorrected model frequencies to compute the frequency ratios as well as the large frequency separation, the latter includes a significant contribution from the surface effect. Assuming that the large frequency separation for the best-fitting model matched reasonably well with the observed separation, the 'true' large separation for the model (excluding the surface effect contribution) is significantly underestimated, and hence the corresponding mean density. This is consistent with previous findings by Silva Aguirre et al. (2017). The internal systematics on the mean density arising from varying the surface correction methods are found to be less than 1.5 per cent.

We note that when one compares the observed frequencies with the uncorrected theoretical frequencies of the best-fitting models obtained using the different surface correction methods, surface corrections should be expected to tend to zero only for low enough frequencies. This is because, assuming that the shape of the surface correction does not match with the differences between the observed and 'true model' frequencies, then the best-fitting model obtained by minimizing the differences between the observed and surface corrected model frequencies would show differences at the

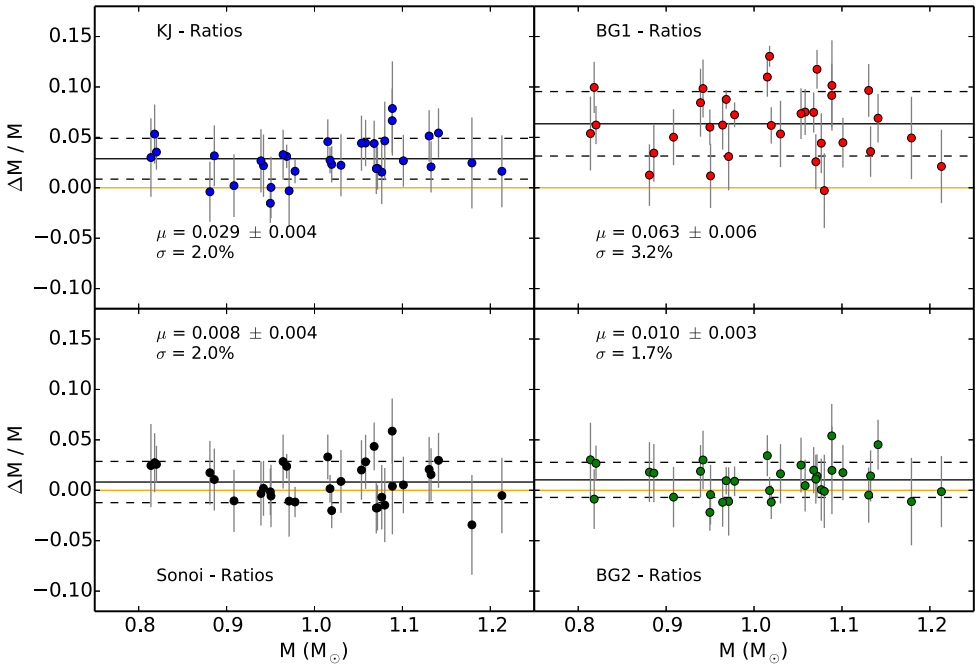

Figure 7. Fractional difference in mass as a function of GS98sta stellar masses. The zero level is represented by the solid orange line. The solid black line indicates the bias (μ), while the scatter (σ) is represented by the dashed lines.

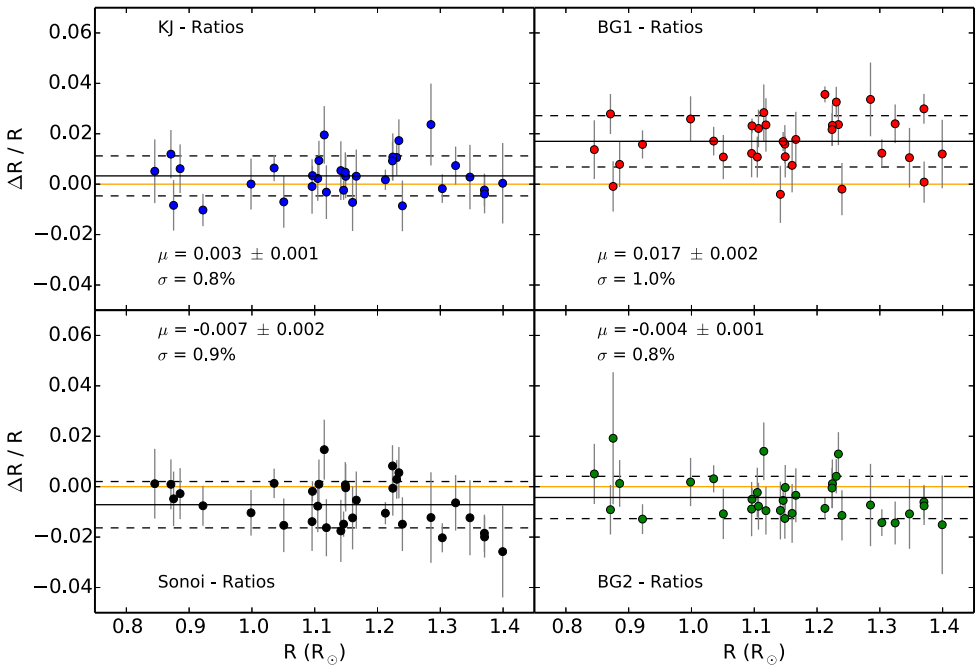

Figure 8. Fractional difference in radius as a function of GS98sta stellar radii. The solid black line indicates the bias (μ), while the scatter (σ) is represented by the dashed lines. The zero level is represented by the solid orange line.

low-frequency end. This arises from how the model frequencies evolve as the model itself evolves. It turns out that if the shape of the assumed surface correction is not correct, then one ends up with either underevolved or overevolved model as the best-fitting model (depending on whether assumed surface correction overcorrects or undercorrects). When only frequency ratios are used as seismic constraints, a much larger difference between the observed and uncorrected theoretical frequencies is obtained at the lower frequency end. This is expected since frequency ratios do not carry information about the surface layers. This has a strong impact on the radius and density. It is for this reason we added the large separation calculated from $l = 0$ mode frequencies.

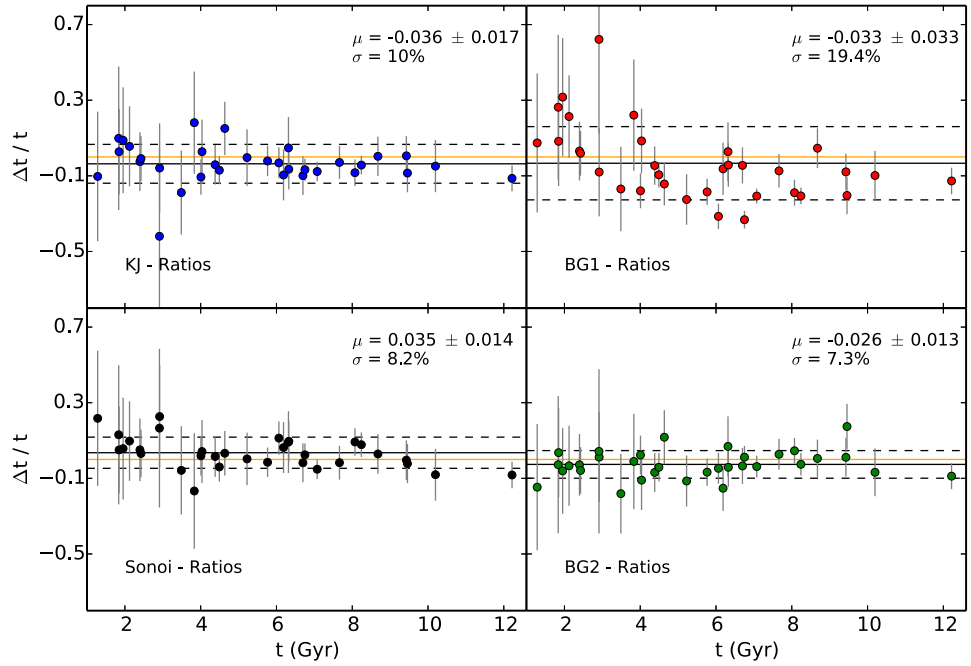

Figure 9. Fractional difference in age as a function of GS98sta stellar ages. The zero level is represented by the solid orange line. The solid black line indicates the bias (μ), while the scatter (σ) is represented by the dashed lines.

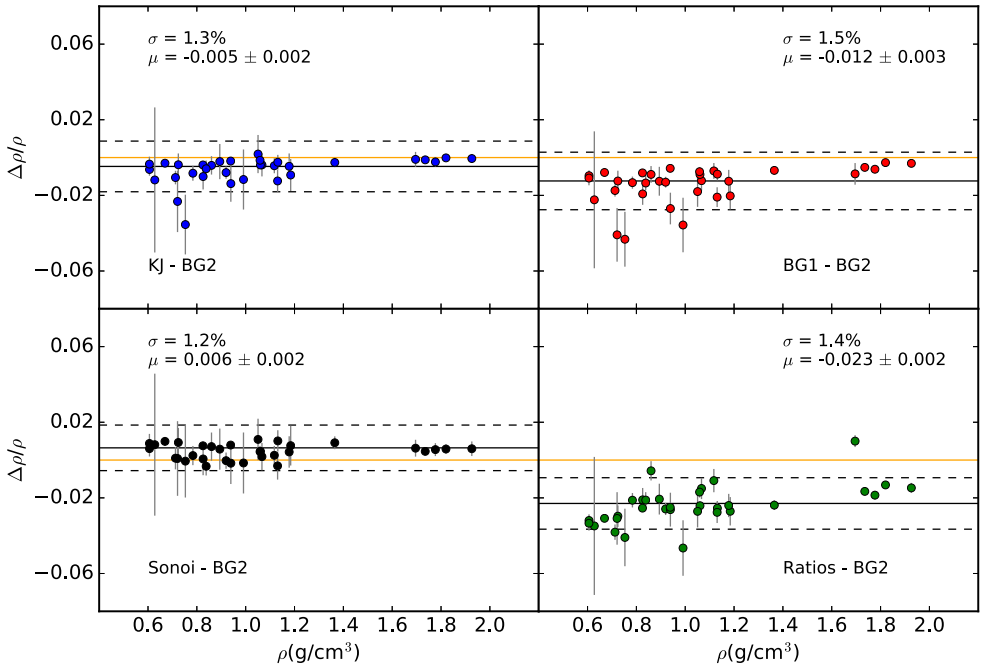

Figure 10. Fractional difference in stellar mean density as a function of GS98sta stellar mean density. The zero level is represented by the solid orange line. The solid black line indicates the bias (μ), while the scatter (σ) is represented by the dashed lines.

5 SUMMARY

We investigated the internal systematics in mean density, radius, mass, and age arising from changes in particular physical aspects of stellar models. We did so based on the analysis of stellar model grids constructed as uniformly as possible and only varying the input physics is being considered. However, internal systematics arising from the uncertainty in solar metallicity mixture will contain contributions from their respective opacities. Moreover, we also assessed the internal systematics arising from the use of different surface correction methods in forward modelling.

We found internal systematics from the uncertainty in solar metallicity mixture to be comparable to the statistical uncertainties. Specifically, we found internal systematics of 0.7 per cent, 0.5 per cent, 1.4 per cent, and 6.7 per cent in mean density, radius, mass, and age, respectively. Relative median statistical uncertainties from using our reference grid (GS98sta) are 0.3 per cent in density,

0.6 per cent in radius, 1.6 per cent in mass, and 7.4 per cent in age. Silva Aguirre et al. (2015) found systematic contributions arising from the uncertainty in solar metallicity mixture to be 0.3 per cent in density and radius, 0.6 per cent in mass, and 3.3 per cent in age. The internal systematics found in this work are approximately twice as large as those found by Silva Aguirre et al. (2015). The most probable cause for this difference is the fact that we treat the mixing length parameter, $\alpha_{\rm mlt,}$ (see Section 4.2) as a free parameter.

Concerning the impact of diffusion, we have shown that the inclusion of diffusion in stellar grids of solar-type stars leads to models with significantly lower ages. This is consistent with previous findings (Silva Aguirre et al. 2015; Dotter et al. 2017). We found internal systematics of 0.5 per cent, 0.8 per cent, 2.1 per cent, and 16 per cent in mean density, radius, mass, and age, respectively. The internal systematics in age are significantly larger than the corresponding statistical uncertainties.

We assessed the impact of using different surface correction methods on the derived stellar parameters. We found the corrections by Sonoi and BG2 yield the least internal systematics, namely, 0.9 per cent and 0.8 per cent in radius, 2.0 per cent and 1.7 per cent in mass, and 8.2 per cent and 7.3 per cent in age, respectively. These internal systematics are comparable to the statistical uncertainties. KJ performs satisfactorily for our sample (see the discussion in Section 4.3), while BG1 yields the largest internal systematics as well as the largest biases for stellar radius and mass. We found stellar masses to be overestimated when using the KJ and BG1 corrections.

Asteroseismology is proving to be particularly significant for the study of solar-type stars, in great part due to the exquisite data that have been made available by NASA's *Kepler* space telescope. The future looks even brighter, with NASA's *TESS* and ESA's PLATO space missions promising to revolutionize the field and increase the number of stars with detected oscillations by several orders of magnitude. The information contained in stellar oscillations allows the internal stellar structure to be constrained to unprecedented levels, while also allowing fundamental stellar properties (e.g. mass, radius, and age) to be precisely determined. In anticipation of the flood of observations from future space missions, a number of the state-of-the-art asteroseismic techniques for the estimation of fundamental stellar properties are currently being developed and tested. Particular attention is being placed on calibrating the determination of age, due to the strong dependence this quantity has on stellar physics. This work therefore provides a valuable contribution to this communal effort by assessing the systematics on the derived stellar properties that arise from specific changes in the model input physics.

ACKNOWLEDGEMENTS

This work was supported by Fundação para a Ciência e a Tecnologia (FCT, Portugal) through national funds (UID/FIS/04434/2013) and by FEDER through COMPETE2020 (POCI-01-0145-FEDER-007672). This work was also financed by FEDER - Fundo Europeu de Desenvolvimento Regional funds through the COMPETE 2020 - Operacional Programme for Competitiveness and Internationalisation (POCI), and by FCT in the framework of the project POCI-01-0145-FEDER-030389. BN is supported by Fundação para a Ciência e a Tecnologia (FCT, Portugal) under the Grant ID: PD/BD/113744/2015 from PHD:SPACE an FCT PhD program. MSC is supported by FCT through an Investigador contract of reference IF/00894/2012 and POPH/FSE (EC) by FEDER funding through the program COMPETE. Funding for the Stellar Astrophysics Centre is provided by The Danish National Research Foundation (grant agreement no.: DNRF106) The authors thank the MESA user community for the engaging conversations about MESA. The AIMS project was developed at the University of Birmingham by Daniel R. Reese as one of the deliverables for the SPACEINN network. The SPACEINN network was funded by the European Community's Seventh Framework Programme (FP7/2007-2013) under grant agreement no. 312844. We thank the reviewer for the constructive remarks.

REFERENCES

Allen C. W., 1976, Astrophysical Quantities, 3rd edn. Athlone Press, London
Aller L. H., Chapman S., 1960, ApJ, 132, 461
Angulo C. et al., 1999, Nucl. Phys. , 656, 3
Asplund M., Grevesse N., Sauval A. J., Scott P., 2009, ARA&A, 47, 481
Ball W. H., Gizon L., 2014, A&A, 568, A123
Ball W. H., Gizon L., 2017, A&A, 600, A128
Balser D. S., 2006, AJ, 132, 2326
Basu S., Antia H. M., 2004, ApJ, 606, L85
Benomar O., Masuda K., Shibahashi H., Suto Y., 2014, PASJ, 66, 94
Borucki W. J. et al., 2010, Science, 327, 977
Brandão I. M. et al., 2011, A&A, 527, A37
Brown T. M., Gilliland R. L., Noyes R. W., Ramsey L. W., 1991, ApJ, 368, 599
Böhm-Vitense E., 1958, Z. Astrophys., 46, 108
Campante T. L., Santos N. C., Monteiro M. J. P. F. G., eds, 2017, in Astrophysics and Space Science Proceedings, Vol. 49, Asteroseismology and Exoplanets: Listening to the Stars and Searching for New Worlds. Springer, Berlin
Campante T. L. et al., 2015, ApJ, 799, 170
Campante T. L. et al., 2016a, ApJ, 819, 85
Campante T. L. et al., 2016b, ApJ, 830, 138
Casagrande L., Flynn C., Portinari L., Girardi L., Jimenez R., 2007, MNRAS, 382, 1516
Casagrande L. et al., 2014, ApJ, 787, 110
Chaboyer B., Fenton W. H., Nelan J. E., Patnaude D. J., Simon F. E., 2001, ApJ, 562, 521
Chiosi C., Matteucci F. M., 1982, A&A, 105, 140
Christensen-Dalsgaard J., Dappen W., Lebreton Y., 1988, Nature, 336, 634
Christensen-Dalsgaard J., Monteiro M. J. P. F. G., Rempel M., Thompson M. J., 2011, MNRAS, 414, 1158
Christensen-Dalsgaard J., Proffitt C. R., Thompson M. J., 1993, ApJ, 403, L75
Christensen-Dalsgaard J., Thompson M. J., 1997, MNRAS, 284, 527
Cyburt R. H., Fields B. D., Olive K. A., 2003, Phys. Lett. , 567, 227
Davies G. R. et al., 2016, MNRAS, 456, 2183
Deheuvels S., Michel E., 2011, A&A, 535, A91
Deheuvels S. et al., 2014, A&A, 564, A27
Dotter A., Conroy C., Cargile P., Asplund M., 2017, ApJ, 840, 99
Dziembowski W. A., Paterno L., Ventura R., 1988, A&A, 200, 213
Ferguson J. W., Alexander D. R., Allard F., Barman T., Bodnarik J. G., Hauschildt P. H., Heffner-Wong A., Tamanai A., 2005, ApJ, 623, 585
Figueira P., Faria J. P., Adibekyan V. Z., Oshagh M., Santos N. C., 2016, Orig. Life Evol. Biosph., 46, 385
Foreman-Mackey D., Hogg D. W., Lang D., Goodman J., 2013, PASP, 125, 306
Goldreich P., Murray N., Willette G., Kumar P., 1991, ApJ, 370, 752
Gough D., 1990, in Osaki Y. , Shibahashi H. , eds, Lecture Notes in Physics, Vol. 367, Progress of Seismology of the Sun and Stars. Springer-Verlag, Berlin , p. 283
Gregory P. C., 2005, Bayesian Logical Data Analysis for the Physical Sciences: A Comparative Approach with 'Mathematical' Support. Cambridge Univ. Press, Cambridge
Grevesse N., Sauval A. J., 1998, Space Sci. Rev., 85, 161
Gruberbauer M., Guenther D. B., MacLeod K., Kallinger T., 2013, MNRAS, 435, 242
Guzik J. A., Cox A. N., 1993, ApJ, 411, 394

Huber D. et al., 2013, ApJ, 767, 127
Iglesias C. A., Rogers F. J., 1996, ApJ, 464, 943
Imbriani G. et al., 2005, Eur. Phys. J. A, 25, 455
Jimenez R., Flynn C., MacDonald J., Gibson B. K., 2003, Science, 299, 1552
Kjeldsen H., Bedding T. R., 1995, A&A, 293, 87
Kjeldsen H., Bedding T. R., Christensen-Dalsgaard J., 2008, ApJ, 683, L175
Korn A. J., Grundahl F., Richard O., Mashonkina L., Barklem P. S., Collet R., Gustafsson B., Piskunov N., 2007, ApJ, 671, 402
Kunz R., Fey M., Jaeger M., Mayer A., Hammer J. W., Staudt G., Harissopulos S., Paradellis T., 2002, ApJ, 567, 643
Lebreton Y., Goupil M. J., 2014, A&A, 569, A21
Lodders K., Palme H., 2009, Meteorit. Planet. Sci. , 72, 5154
Lund M. N. et al., 2017, ApJ, 835, 172
Maeder A., Meynet G., 2000, ARA&A, 38, 143
Mamajek E. E., 2012, ApJ, 754, L20
Marcy G. W. et al., 2014, ApJS, 210, 20
Mathur S. et al., 2012, ApJ, 749, 152
Metcalfe T. S. et al., 2010, ApJ, 723, 1583
Metcalfe T. S. et al., 2012, ApJ, 748, L10
Metcalfe T. S. et al., 2014, ApJS, 214, 27
Miglio A., Montalbán J., 2005, A&A, 441, 615
Monteiro M. J. P. F. G., Christensen-Dalsgaard J., Thompson M. J., 1996, A&A, 307, 624
Mosser B. et al., 2013, A&A, 550, A126
Nsamba B., Monteiro M. J. P. F. G., Campante T. L., Reese D. R., White T. R., García Hernández A., Jiang C., 2017, EPJ Web Conf., 160, 05010
Paxton B., Bildsten L., Dotter A., Herwig F., Lesaffre P., Timmes F., 2011, ApJS, 192, 3
Paxton B. et al., 2013, ApJS, 208, 4
Paxton B. et al., 2015, ApJS, 220, 15
Perryman M., 2014, The Exoplanet Handbook. Cambridge Univ. Press, Cambridge
Piau L., Kervella P., Dib S., Hauschildt P., 2011, A&A, 526, A100
Pinsonneault M. H., An D., Molenda-Żakowicz J., Chaplin W. J., Metcalfe T. S., Bruntt H., 2012, ApJS, 199, 30
Pinsonneault M. H. et al., 2014, ApJS, 215, 19
Ramírez I., Meléndez J., Asplund M., 2009, A&A, 508, L17
Rauer H. et al., 2014, Exp. Astron., 38, 249
Rogers F. J., Nayfonov A., 2002, ApJ, 576, 1064
Roxburgh I. W., Vorontsov S. V., 2003, A&A, 411, 215
Serenelli A. M., Basu S., 2010, ApJ, 719, 865
Silva Aguirre V., Ballot J., Serenelli A. M., Weiss A., 2011, A&A, 529, A63
Silva A guirre V. et al., 2013, ApJ, 769, 141
Silva A guirre V. et al., 2015, MNRAS, 452, 2127
Silva A guirre V. et al., 2017, ApJ, 835, 173
Sonoi T., Samadi R., Belkacem K., Ludwig H.-G., Caffau E., Mosser B., 2015, A&A, 583, A112
Thoul A. A., Bahcall J. N., Loeb A., 1994, ApJ, 421, 828
Townsend R. H. D., Teitler S. A., 2013, MNRAS, 435, 3406
Trampedach R., Stein R. F., 2011, ApJ, 731, 78
Trampedach R., Stein R. F., Christensen-Dalsgaard J., Nordlund Å., Asplund M., 2014, MNRAS, 445, 4366
Turcotte S., Richer J., Michaud G., Iglesias C. A., Rogers F. J., 1998, ApJ, 504, 539
Valle G. et al., 2014, A & A, 561:A125
Valle G. et al. 2015, A & A, 575:A12
VandenBerg D. A., Richard O., Michaud G., Richer J., 2002, ApJ, 571, 487
Van Eylen V., Kjeldsen H., Christensen-Dalsgaard J., Aerts C., 2012, Astron. Nachr., 333, 1088
White T. R. et al., 2017, A&A, 601, A82

This paper has been typeset from a TEX/LATEX file prepared by the author.